3-D Printed Metal-Pipe Rectangular Waveguides

Mario D'Auria, *Student Member, IEEE*, William J. Otter, *Member, IEEE*, Jonathan Hazell, Brendan T. W. Gillatt, Callum Long-Collins, Nick M. Ridler, *Fellow, IEEE*, and Stepan Lucyszyn, *Fellow, IEEE*

***Abstract*— This paper first reviews manufacturing technologies for realizing air-filled metal-pipe rectangular waveguides (MPRWGs) and 3-D printing for microwave and millimeter-wave applications. Then, 3-D printed MPRWGs are investigated in detail. Two very different 3-D printing technologies have been considered: low-cost lower-resolution fused deposition modeling for microwave applications and higher-cost high-resolution stereolithography for millimeter-wave applications. Measurements against traceable standards in MPRWGs were performed by the U.K.'s National Physical Laboratory. It was found that the performance of the 3-D printed MPRWGs were comparable with those of standard waveguides. For example, across X-band (8–12 GHz), the dissipative attenuation ranges between 0.2 and 0.6 dB/m, with a worst case return loss of 32 dB; at W-band (75–110 GHz), the dissipative attenuation was 11 dB/m at the band edges, with a worst case return loss of 19 dB. Finally, a high-performance W-band sixth-order inductive iris bandpass filter, having a center frequency of 107.2 GHz and a 6.8-GHz bandwidth, was demonstrated. The measured insertion loss of the complete structure (filter, feed sections, and flanges) was only 0.95 dB at center frequency, giving an unloaded quality factor of 152—clearly demonstrating the potential of this low-cost manufacturing technology, offering the advantages of lightweight rapid prototyping/manufacturing and relatively very low cost when compared with traditional (micro)machining.**

***Index Terms*— 3-D printing, additive manufacturing, fused deposition modeling (FDM), metal-pipe rectangular waveguide (MPRWG), rapid manufacturing, rectangular waveguide, stereolithography apparatus (SLA).**

I. Introduction

THE relatively very low loss characteristics of conventional metal-pipe rectangular waveguides (MPRWGs), compared with planar transmission lines (e.g., coplanar waveguide or microstrip), make this technology essential for applications where dissipative attenuation is a critical factor.

Manuscript received May 21, 2015; revised July 15, 2015; accepted July 22, 2015. Date of publication August 20, 2015; date of current version September 18, 2015. This work was supported by the Innovative Electronics Manufacturing Research Centre through the U.K. Engineering and Physical Sciences Research Council Project entitled 3-D Microwave and Millimeter-Wave System-on-Substrate Using Sacrificial Layers for Printed RF MEMS Component under Grant SP/02/03/10. Recommended for publication by Associate Editor A. Shapiro upon evaluation of reviewers' comments.

M. D'Auria, W. J. Otter, J. Hazell, B. T. W. Gillatt, C. Long-Collins, and S. Lucyszyn are with the Optical and Semiconductor Devices Group, Imperial College London, London SW7 2AZ, U.K. (e-mail: m.dauria10@imperial.ac.uk; w.otter@imperial.ac.uk; jonathan.hazell08@imperial.ac.uk; brendan.gillatt10@imperial.ac.uk; callum.long-collins09@imperial.ac.uk; s.lucyszyn@imperial.ac.uk).

N. M. Ridler is with the Time, Quantum and Electromagnetics Division, National Physical Laboratory, Middlesex TW11 0LW, U.K. (e-mail: nick.ridler@npl.co.uk).

Color versions of one or more of the figures in this paper are available online at http://ieeexplore.ieee.org.

Digital Object Identifier 10.1109/TCPMT.2015.2462130

The manufacturing cost for complex 3-D structures represents a limitation for low-cost applications; this is exacerbated when frequency increases into the millimeter-wave band, due to the more demanding requirements in mechanical precision for smaller feature sizes. For this reason, alternative enabling technologies have been explored for their manufacture. For example, for monolithic microwave integrated circuits, surface micromachined dielectric-filled MPRWGs were demonstrated in [1] and [2] in W-band (75 to 110 GHz) at 105 GHz. This concept was then adapted to low-cost thick-film processing on ceramic substrates and demonstrated from 60 to 90 GHz [3]. A more recent innovation that readily supports tunable components and reconfigurable architectures employs the use of 2-D and 3-D metamaterials (holey metal surface and wire media, respectively) with demonstrators at X-band (8–12 GHz) [4]. Advanced reconfigurable substrate-integrated waveguide architectures for terahertz applications were proposed in [5], with the use of *virtual* sidewalls within high-resistivity silicon wafers, patterned by programmable laser light sources. Unfortunately, these alternative manufacturing technologies can result in much higher dissipative losses.

Commercial MPRWGs are traditionally manufactured by reshaping (drawing) metal pipes through rectangular dies or from machining by either computerized numerically controlled (CNC) milling or electronic discharge machining (EDM) with spark erosion. For convenience, these will be classified as machining technologies. A state-of-the-art CNC machined split-block WR-10 band (75–110 GHz) thru line waveguide in aluminum was reported with an average attenuation of 4-dB/m across W-band [6]. Chemically polished copper EDM WR-10 waveguides have also been measured with the same level of attenuation [7].

In contrast, micromachining technologies can include bulk micromachining of silicon [8]–[12] and surface micromachining of dielectrics [1], [2] or photoresist layers [13]–[22]. Silicon micromachined MPRWGs are of particular interest for (sub-)millimeter frequencies. For example, a gold-plated WR-10 waveguide has a reported measured attenuation of 0.05 dB/λ_g at 100 GHz [8]. A similarly WR-1.5 band (500–750 GHz) waveguide was recently reported with attenuation of ~80 dB/m at 600 GHz [12].

The pioneering work reported in [13] demonstrated the use of X-ray photoresist lithography for the manufacture of waveguides for terahertz applications. The following year, this concept was developed further by Collins *et al.* with standard photolithography using SU-8 photoresist as the sacrificial building material for the manufacture of air-filled waveguides

and slotted H-plane sectoral horn antennas in W-band, G-band (140–220 GHz) and at 1.6 THz [14]–[17]. This work was undertaken within the U.K.'s EPSRC-funded research program Terahertz Integrated Technology Initiative (TINTIN). It is also interesting to note that the TINTIN consortium first reported the concept of SU-8 formed split-block waveguides, using their snap-together techniques, demonstrating a loss of $\sim$0.5 dB/λ_g at W-band [15]. More recently, Smith *et al.* [18] have demonstrated WR-3.4 band (220–330 GHz) split-block waveguides and cylindrical cavities. The most recently reported work on SU-8 formed split-block waveguides, from the University of Birmingham (U.K.), also showed impressive results at 60 GHz [19], 280 GHz [20], [21], and 650 GHz [22].

Machining and micromachining technologies are relatively expensive manufacturing solutions. A low-cost alternative for the manufacture of MPRWGs is to use micromolding (which include injection molding and hot embossing), followed by a traditional metal plating process. WR-10 gold electroplated plastic waveguides [23] and filters [24] have been reported. The former demonstrated a worst case return loss of 14-dB across W-band and a minimum attenuation of 0.116 dB/λ_g (or 27.6 dB/m) at 92.5 GHz [23]. The associated fifth-order inductive iris filter demonstrated a worst case passband return loss of 12 dB and attenuation of 3.49 dB at 95.4 GHz [24].

Over the past two decades, 3-D printing (also known as additive manufacturing) has found widespread applications in rapid prototyping and manufacturing of high geometrical complexity components. Academic interest in microwave and millimeter-wave research began at the University of Michigan Ann Arbor in 2002, with the development of metamaterials and electromagnetic bandgap (EBG) structures in ceramics, by either coextrusion or casting in stereolithographically made molds. This research was led by Chappell and Katehi [25]–[27]. In 2004, they went on to investigate microwave passive components (e.g., cylindrical and rectangular air-filled cavity resonators, and nonplanar helical and monopole antennas) and coupled-cavity resonator filters [28]–[30]. This pioneering work on stereolithography included K_u-band (12–18 GHz) horn antennas in [31].

Ceramic stereolithography was used to develop dielectric antennas in [32]–[34] and photonic crystal waveguides in [35] and [36]. At the same time, within Europe, XLIM—UMR CNRS at the University of Limoges used ceramic (micro)stereolithography for the fabrication of microwave filters, antennas, and millimeter-wave EBG crystals [37]–[40].

Over the past eight years, further examples of 3-D printed microwave and millimeter-wave components have been reported: 1) metamaterials [41]–[43]; 2) corrugated and dielectric-filled horn antennas [44], [45]; 3) patch antennas [46], [47]; 4) graded index and Luneburg lenses [48], [49]; and 5) frequency selective surfaces [50]. At terahertz frequencies, EBG structures, plasmonic and hollow core wire waveguides, and dielectric reflectarray antennas [51]–[55].

Apart from the early examples, by Chappell's group in 2004 and 2005, of 3-D printed air-filled MPRWG components: e.g., cavity resonators [28]–[30], filters [29], and WR-62 band (12.4–18 GHz) pyramidal horn antennas [31], little has been reported in the open literature. Notable exceptions include a 35–39.5 GHz dielectric-filled horn antenna array in [44] and the W-band air-filled MPRWG (and circular waveguide corrugated horn antenna) in [45].

Recently, in 2012, the Swiss Federal Institute of Technology in Lausanne and its spin-off company (Swissto12) reported the 3-D printing of passive structures for millimeter-wave and terahertz applications in their short note [56]. More recently, since 2014, Swissto12 have been advertising 3-D printed metal-coated plastic (MCP) waveguides and diagonal pyramidal horn antennas [57], [58]. These air-filled MPRWGs operate in the WR-3.4 band and, with copper metallization, have a reported minimum attenuation of 12 dB/m at *ca.* 280 GHz. In addition, WR-5.1 band (140–220 GHz) MCP waveguides are also commercially available in both straight and with S-bend sections.

With all the examples of stereolithographic 3-D printing [25]–[58], little detail is given on the metrology for determining performance. Moreover, to date, the lower cost 3-D printing technology that exploits plastic extrusion techniques has not been reported for microwave rectangular waveguide applications. In this paper, the 3-D printing of X-band and W-band MPRWGs using plastic extrusion (thermoplastic deposition) and stereolithographic (UV resin curing) techniques, respectively, are compared and contrasted. In addition, a high-performance W-band inductive iris bandpass filter is reported. All measurements are traceable to national standards in MPRWGs, performed by the U.K.'s National Physical Laboratory (NPL).

II. 3-D Printing Technologies and Metallization

3-D printing is based on layer-by-layer material deposition to realize arbitrary 3-D objects. Different 3-D printer technologies are commercially available. They can be classified into three main categories: 1) selective deposition of extruded material, which includes fused deposition modeling (FDM) [59]; 2) UV curing of resin, which includes inkjet printing and stereolithography apparatus (SLA) technology [60]; and 3) powder binding, which includes selective laser sintering (SLS) [61]. Within the scope of this paper, the first two (specifically, FDM and SLA) will be considered further.

A. Fused Deposition Modeling Technology

Injection molding is by far the cheapest fabrication technology when high-volume manufacturing is required. However, the cost of the mold can be very expensive and there are practical limitations on geometry for 3-D structures. As an alternative for rapid manufacturing, there is increasing interest in FDM 3-D printing; comparative case studies have been reported [62]–[66]. In general, since the unit cost with 3-D printing is relatively constant with volume, while the cost of injection molding falls sharply, a break point in total manufacturing costs exists at low volumes. Moreover, 3-D printing can be used to realize be-spoke components with highly complex geometries.

FDM printing is based on extrusion and selective deposition of thermoplastics. With this technology, the

smallest achievable feature size on the horizontal xy plane is limited by the extrusion nozzle aperture; for example, having a typical diameter of 400 μm. Along the vertical build z-axis, feature size is limited by the minimum repeatable mechanical displacement, typically between 50 and 100 μm. As a result, the typical voxel size is of the order of $400 \times 400 \times 50$ μm^3.

Solid objects are usually partially hollow, having a solid shell that defines the outer geometry and internal support scaffold for additional rigidity. The walls of the printed object will have visible scallops in the vertical direction; the extent of which is dependent on the chosen layer height. Scallops are caused by the melted thermoplastic assuming a circular shape.

B. Stereolithography Apparatus Technology

With SLA 3-D printing, a photosensitive resin is contained within a tank. The top of the tank is scanned with a UV laser, which selectively cures the top layer of resin. The 3-D printed object sits on a platform within the tank. After one layer has been cured, the platform is lowered and a fresh layer of resin is poured in front of the squeegee and leveled off by the squeegee; the whole process is then repeated. Finally, the part is rinsed of excess resin and then fully cured in a UV oven.

When compared with FDM printing, the small spot size of the laser and the low viscosity of the resin allow for much smoother surfaces, resulting in a greatly reduced minimum feature sizes in all directions, resulting in a typical voxel size of $50 \times 50 \times 50$ μm^3. While greater resolution can be achieved, the capital equipment and running costs are significantly greater than those associated with FDM printing.

C. Electroless Plating

Unlike FDM and SLA, with SLS it is possible to 3-D print solid metal structures [61]; albeit having relatively poor electrical conductivity and, therefore, high dissipative losses for microwave and millimeter-wave applications. In practice, this very expensive manufacturing technology is usually reserved for be-spoke applications where metal casting or CNC machining is impractical.

The two very different 3-D printing technologies considered here can create arbitrary 3-D structures, but in general only from lossy dielectric building materials (plastic with FDM and resin with SLA). As a result, to create MPRWG structures, the dielectric material is only used here as a structural support for the internal MPRWG walls. This process is then followed by metal plating to realize the air-filled structure.

A standard commercial electroless metal plating process was employed. Here, the dielectric structure is sequentially immersed in a series of chemical baths for surface preparation, surface activation (with a catalyst), and metal deposition [67]. With optimal conditions, this technique is able to uniformly coat the entire surface of the structure with a seed layer, which can then be electroplated with the desired metal having a thickness that greatly exceeds five skin depths.

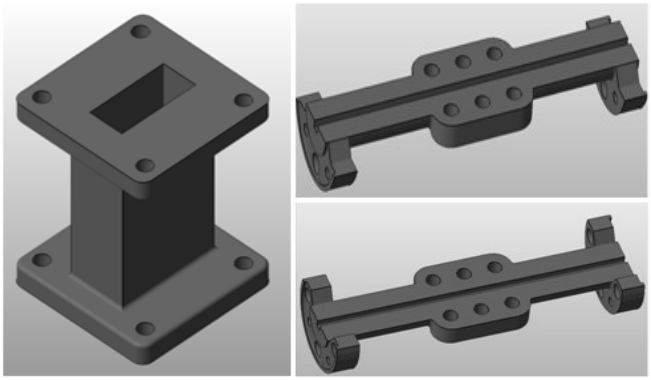

(a) (b)

Fig. 1. CAD designs for 3-D printable MPRWG thru lines. (a) Single piece WR-90 compatible. (b) Split-block WR-10 compatible.

III. 3-D Printed Metal-Pipe Rectangular Waveguides

The MPRWGs were originally designed to be compatible with standard flanges and waveguides [UBR100 flanges with WR-90 band (8.2–12.4 GHz) waveguides for X-band and anticocking UG-387/U-M flanges with WR-10 waveguides for W-band]. The calculated midband insertion loss for ideal waveguides having pure copper internal walls are 0.108 dB/m at 10 GHz for WR-90 and 2.69 dB/m at 90 GHz for WR-10 [68]. Obviously, assuming copper walls, the measured insertion loss for commercially available waveguides is expected to be higher than these theoretical lower bound values.

For manufacturing the larger X-band waveguide structures, FDM technology was employed, as it represents a lower cost solution; the larger voxel size and mechanical positioning repeatability may be considered to be within acceptable manufacturing tolerances for many microwave applications. With the metal plating process, for WR-90, the internal dimensions are sufficiently large to avoid regions of depleted solute within the chemical solutions inside the waveguide structure. As a result, the MPRWG components can be designed as a single-piece structure. An illustration of a WR-90-compatible thru line design is given in Fig. 1(a).

An entry-level desktop 3-D printer was used (Makerbot Replicator 2X) with acrylonitrile butadiene styrene (ABS) as the building material. The 3-D printer software cuts the CAD drawing of a solid structure into horizontal slices and translates each slice into a 2-D path for the nozzle head to follow. The operator must first define three parameters: 1) surface wall thickness (1 mm in our case) along the x, y, and z axes; 2) infill percentage between surface walls for the hexagonal (honeycomb) scaffolding in the xy plane, along the z-axis (10% in our case); and 3) layer resolution along the z-axis (100 μm in our case). With our designs, the total thickness of the waveguide walls (i.e., distance between surface walls) was 6 mm. After printing, electroless plating of a 3-μm-thick nickel seed layer was performed, followed by the electroplating of a 27-μm-thick layer of copper. The resulting manufactured thru line is shown in Fig. 2. The weights

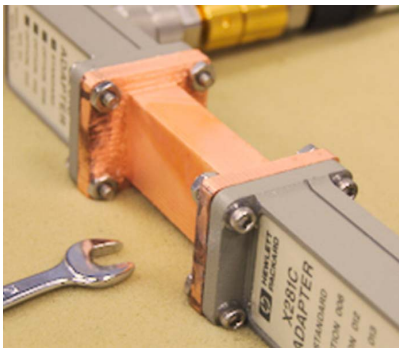

Fig. 2. 3-D printed and copper-plated WR-90 thru line between commercial measurement test heads.

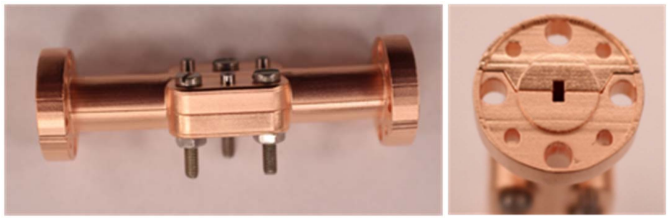

(a) (b)

Fig. 3. 3-D printed and copper-plated WR-10 thru line after assembly of the split block. (a) and (b) Side-view and end-view showing the self-aligned flange.

for each individual postplated flange and waveguide are 5.9 g and 250 mg/mm, respectively. Comparable waveguide components commercially available within our laboratory have corresponding values of 7.5 g and 730 mg/mm. Clearly, there is a considerable weight advantage in 3-D printing X-band waveguides.

For manufacturing the smaller W-band waveguide structures, SLA technology was employed, as the smaller voxel size and higher mechanical accuracy of the laser galvo-scanner are required to meet the more demanding manufacturing tolerances of both flanges and waveguides. In contrast to WR-90, the internal dimensions of a single-piece WR-10 structure are too small to give acceptable metal plating. As a result, a split-block solution was adopted. To minimize radiation losses, the break was along the E-plane and located at the center of the broad wall. In principle, SLA technology allows for good mechanical alignment of the two halves. An illustration of a WR-10-compatible thru line design is given in Fig. 1(b).

The solid SLA printed parts were fabricated using a 3-D Systems Viper si2 with Accura Xtreme resin [69] as the building material. This professional-level system offers a minimum focused laser beam spot diameter of 25 μm and a layer resolution of 25 μm. After printing, the same electroless plating and electroplating processes were performed as with the previous WR-90 waveguide components. The assembled manufactured thru line is shown in Fig. 3. A small amount of warping of the two individual parts of the MPRWG was observed along its longitudinal direction. It is believed that warping is due to the built-in stresses that are created when the structure undergoes final curing in a UV oven. However, with our self-aligning design for the two individual split-block parts, no noticeable warping in the final assembled components was observed.

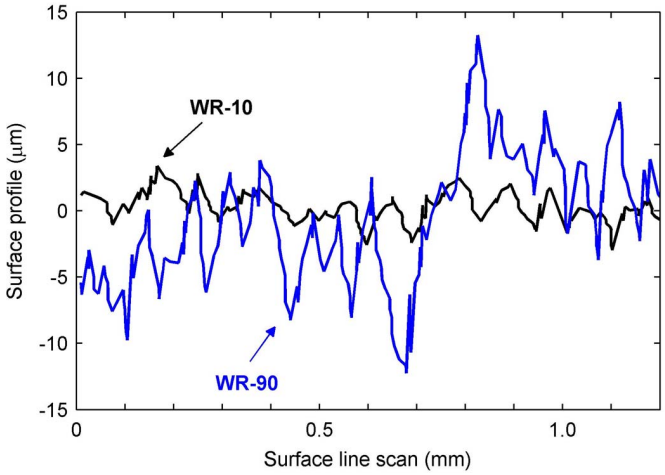

Fig. 4. Measured postplating surface profile scan lines in the z-direction for both WR-90- and WR-10-compatible waveguides.

IV. Internal Surface Roughness Analysis

With both X-band and W-band MPRWGs, after plating, the surface profile of the inner waveguide walls was measured using a Veeco Wyco NT9100 optical surface profiler. A scan line in the z-direction represents the worst case condition, due to scalloping associated with 3-D printing; the measured results are shown in Fig. 4. With FDM printing, the lower layer deposition resolution and poor nozzle positioning repeatability cause significant levels of surface roughness (observed relative peak values are ± 13 μm) and steps (observed relative values are ± 3 μm), respectively. In contrast, as expected, SLA printing performs much better (observed relative peak values of surface roughness are ± 3 μm and without noticeable steps). The average surface roughness values, defined as the arithmetic average of the absolute values of the profile height deviations from the mean line [70], are calculated to be 4.02 and 0.93 μm with FDM and SLA printing, respectively. The root mean square surface roughness values, defined as the square root of the arithmetic average of the squared values of the profile height deviations from the mean line [70], are 4.99 and 1.16 μm with FDM and SLA printing, respectively. It can be seen that with our manufacturing technologies, when compared to FDM, SLA printing offers $\sim$4:1 reduction in surface roughness.

V. Traceable VNA Measurement Methodology

Traceable scattering (S)-parameter measurements were carried out at the U.K.'s NPL. A HP8510C vector network analyzer (VNA) was configured for use with either WR-90 or WR-10 commercial waveguide test heads, covering the complete X-band or W-band, respectively. Thru-reflect-line (TRL) calibration [71] was first performed, using short circuit and 90° delay primary standards; the test head flanges

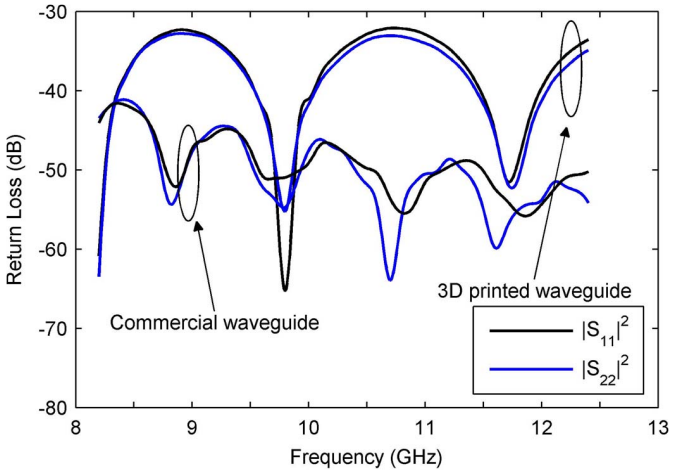

Fig. 5. Measured return losses for the 60-mm length FDM printed and 127-mm length commercial machined WR-90 reference thru line waveguides.

define the two-port measurement reference planes. An in-house calibration algorithm was employed, having a seven-term error-correction model [72]. The overall setup (VNA, primary standards and calibration algorithm) is referred to as the NPL Primary Impedance Microwave Measurement System (PIMMS) [73], [74]. This is the U.K.'s primary national standard system for S-parameter measurements.

For each individual 3-D printed and commercial machined (copper alloy WR-90 and aluminum WR-10, the latter taken from a Hewlett Packard VNA verification kit) reference thru line waveguide component, six measurements were taken; each measurement was preceded by a TRL calibration. The calibrated measurements were then processed by the PIMMS software to calculate the average results. This approach was chosen to reduce the influence of flange connection repeatability, cable flexing, system noise, and changes in the ambient environment. As a result, the standard error of the arithmetic mean is reduced, giving greater confidence in the measured results for these proof-of-principle demonstrators.

VI. Measured S-Parameter Results

With WR-90, having standard internal cross-sectional dimensions of $a = 22.86$ mm and $b = 10.16$ mm, the lengths of reference thru lines were 60 and 127 mm for the FDM printed copper-walled and commercial machined copper-alloy walled waveguides, respectively. Fig. 5 shows the measured return loss results across X-band. It can be seen that with a worst case return loss of 32 dB the FDM printed MPRWG has excellent impedance matching. With the commercial machined waveguide, the 41 dB worst case return loss performance can be attributed to the reduced alignment errors associated with its flanges (having higher precision in the position and diameter of the alignment/fastening holes). The almost identical and textbook return loss performances at both ports, seen in Fig. 5, indicates good manufacturing tolerances for the FDM printed waveguide flanges.

With uniform sections of MPRWG thru line, total power attenuation $\alpha_T = \alpha_R + l\alpha_D{}'$ [dB] for a given physical length l [m] is due to impedance mismatch reflection losses α_R [dB] at the flange and dissipative (or ohmic) losses $\alpha_D{}'$ [dB/m] associated with the internal metal walls, with [75]

$$\alpha_R = -10 \cdot \log_{10}(1 - |S_{11}|^2) \text{ [dB]} \tag{1}$$

$$\alpha_D{}' = \begin{cases} -\dfrac{10}{l} \cdot \log_{10}\left(\dfrac{|S_{21}|^2}{1 - |S_{11}|^2}\right) \text{ [dB/m]} & \text{(2a)} \\ -\dfrac{10\lambda_g}{l} \cdot \log_{10}\left(\dfrac{|S_{21}|^2}{1 - |S_{11}|^2}\right) \text{ [dB/}\lambda_g\text{]} & \text{(2b)} \end{cases}$$

where λ_g is the guided wavelength; S_{11} and S_{21} are the measured input voltage-wave reflection coefficient and forward voltage-wave transmission coefficient, respectively. In general, (2a) is normally associated with feed lines and interconnects having arbitrary lengths, while (2b) is more appropriate for comparing distributed-element components of specific electrical length (e.g., $\lambda_g/4$ transformers and $\lambda_g/2$ resonators).

Since a designer can control α_R, given a stable manufacturing process, only α_D reflects the quality of a given manufacturing technology. Moreover, since α_R is negligible with our components it will not be considered further. Note that after visual inspection of the assembled components and detailed numerical electromagnetic simulations, radiation losses associated with gaps between flanges or between the two halves of the split-block parts were considered insignificant.

The measured dissipative attenuation results, using (2), are shown in Fig. 6. With the FDM printed waveguide, the worst case dissipative attenuation across the whole of X-band is only 0.017 dB/λ_g (or 0.58 dB/m). At 10 GHz, the dissipative attenuation is 0.33 dB/m, which is significantly more than the calculated value of 0.108 dB/m for the ideal copper WR-90 waveguide [68]. By comparison, the commercial machined waveguide has worst case dissipative attenuation of 0.020 dB/λ_g (or 0.33 dB/m); at 10 GHz, the value of 0.30 dB/m is again still significantly higher than that calculated for the ideal copper waveguide. Nevertheless, the performance of the FDM printed waveguide is better below *ca.* 10 GHz, when compared to our commercial machined waveguide; above *ca.* 10 GHz, the higher dissipative attenuation is thought to be due to the increased levels of surface roughness with the internal copper walls of the 3-D printed MPRWG.

With WR-10, having standard internal cross-sectional dimensions of $a = 2.54$ mm and $b = 1.27$ mm, the lengths of reference thru lines were 60 and 50 mm for the SLA printed copper-walled and commercial machined aluminum-walled waveguides, respectively.

With the original flange design, as shown in Fig. 3(b), a large midband peak in attenuation (and corresponding degradation in return loss) performance was observed. This was extensively investigated using CST Microwave Studio®. It was found that there was unexpected electromagnetic coupling into an air-filled ring cavity, formed between the SLA printed and commercial machined anticocking flanges. To suppress this unwanted resonance, the anticocking flange cavities with the FDM printed waveguide were filled with an electrically conducting compound [the recipe for this compound

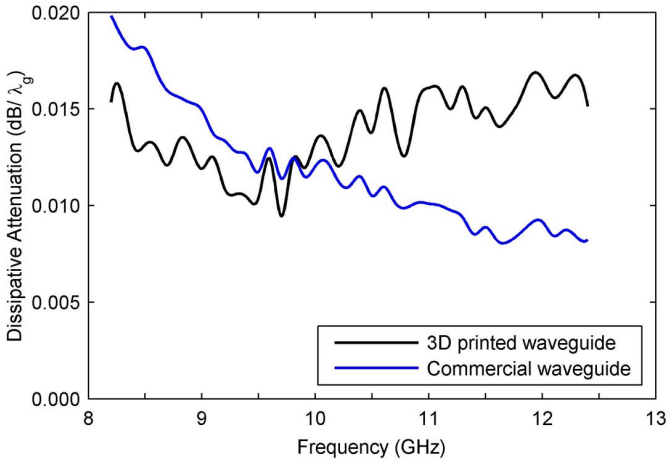

(a)

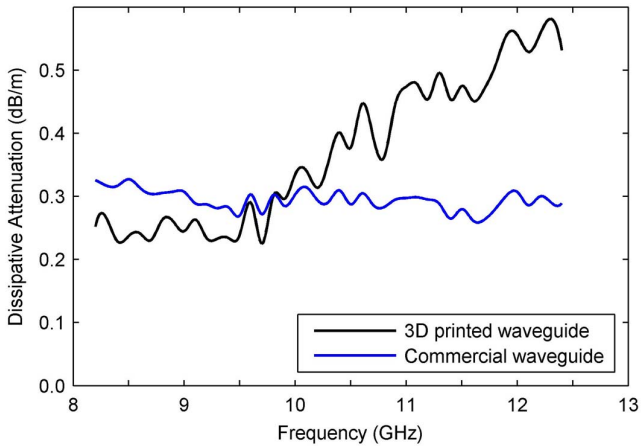

(b)

Fig. 6. Measured dissipative attenuation for the 60-mm length FDM printed waveguide with copper walls and 127-mm length commercial machined WR-90 waveguides with copper alloy walls (a) per guided wavelength and (b) per meter.

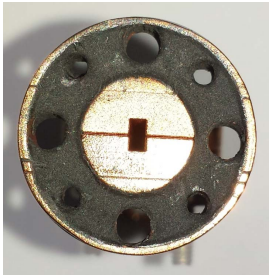

Fig. 7. SLA printed waveguide flange with conducting compound filler.

consisted of 0.65 g of commercial polyvinyl-acetate (PVA) glue, 0.2 g of graphite powder (with average particle size of 10 μm), 3 g Pd/Ag conductive paste (DuPont 6143), and 0.5 g of ready-mix joint filler]. This compound results in an easily workable, high-viscosity paste, having an electrical conductivity of 430 S/m after a setting time of 2 h at 40 °C.

The improved flange is shown in Fig. 7. In addition, flat flanges were created at both test heads by inserting two calibrated shims (2.00 and 3.08 mm in length) from a VNA verification kit. The insertion loss of the two W-band

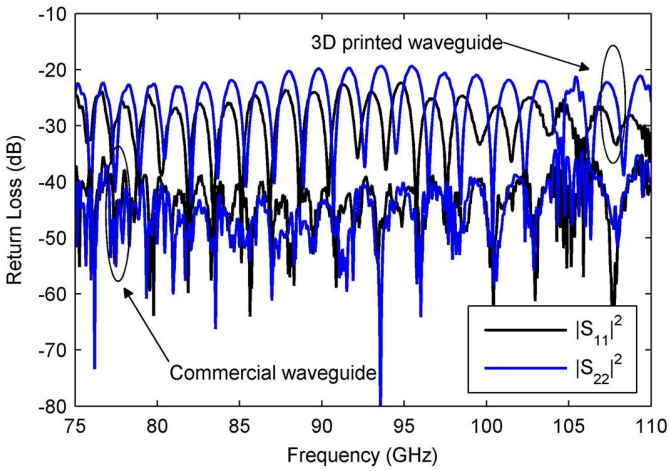

Fig. 8. Measured return loss for the 60-mm length SLA printed and the 50-mm length commercial machined waveguides.

shims was measured separately and found to be negligible. As a result, de-embedding was not considered necessary.

Fig. 8 shows the measured return loss results across W-band. It can be seen that with a worst case return loss of 19 dB the SLA printed MPRWG still has good impedance matching. With the commercial machined waveguide, the 34 dB worst case return loss performance can be attributed to the greatly reduced alignment errors associated with its flanges. The almost identical and textbook return loss performances at both ports indicate good manufacturing tolerances for the commercial machined waveguide flanges. With 3-D printing, our W-band flanges did not perform as well as the X-band flanges, due to the increased accuracy requirements needed for the order of magnitude decrease in waveguide cross section and the choice of split-block solution.

The measured dissipative attenuation results are shown in Fig. 9. With the SLA printed waveguide, the dissipative attenuation increases from ∼11 dB/m at the band edges to a midband peak of 17 dB/m (or 0.07 dB/λ_g).

An iteration in the design and manufacture of the W-band flanges can eliminate the need for the conducting compound filler and introduction of shims. Moreover, since complex geometries can be 3-D printed in a single run, the number of flanges needed within a subsystem can be minimized.

At 110 GHz, the dissipative attenuation of 11 dB/m is significantly greater than the calculated value of 2.69 dB/m at 90 GHz for the ideal copper WR-10 waveguide [68]. Nevertheless, at 110 GHz, the dissipative attenuation of 0.036 dB/λ_g (or 11 dB/m) is commensurate with the commercial machined aluminum waveguide performance of 0.032 dB/λ_g (or 10 dB/m) shown in Fig. 9 and much better than the micromolded waveguide having 0.116 dB/λ_g (or 27.6 dB/m) at 92.6 GHz [23].

A comparison of measured dissipative attenuation results for MPRWGs realized using different manufacturing technologies is given in Table I. It should be noted that this table does not represent an exhaustive survey of what can be found in the open literature, but acts as a useful guide.

TABLE I
COMPARISON OF PUBLISHED MPRWG MEASURED ATTENUATION PERFORMANCES

Waveguide Band	Frequency (GHz)	Manufacturing Technology	Split block	Waveguide Filler	Attenuation dB/m	Attenuation dB/λ_g	References
WR-90	10	Machined	no	air	0.30	0.012	-
WR-90	10	3D printed (FDM)	no	air	0.33	0.013	This work
WR-12	60-80	Thick-film printing	no	HIBRIDAS HD 1000	< 890	-	[3]
WR-10	92.5	Micro molding	no	air	27.6	0.116	[23]
WR-10	100	Bulk micromachined silicon	yes	air	13.5*	0.05	[8]
WR-10	105	Surface micromachining	no	polyimide	8,660	44	[1]-[2]
WR-10	75-110	CNC machined	yes	air	4	-	[6]
WR-10	75-110	Surface micromachined	yes	air	-	0.5	[15]
WR-10	110	Machined	no	air	10	0.032	-
WR-10	110	3D printed (SLA)	yes	air	11	0.036	This work
WR-3.4	280	3D printed	yes	air	12	0.016*	[57]-[58]
WR-1.5	600	Bulk micromachined silicon	yes	air	80	0.053*	[12]

*calculated values using (2)

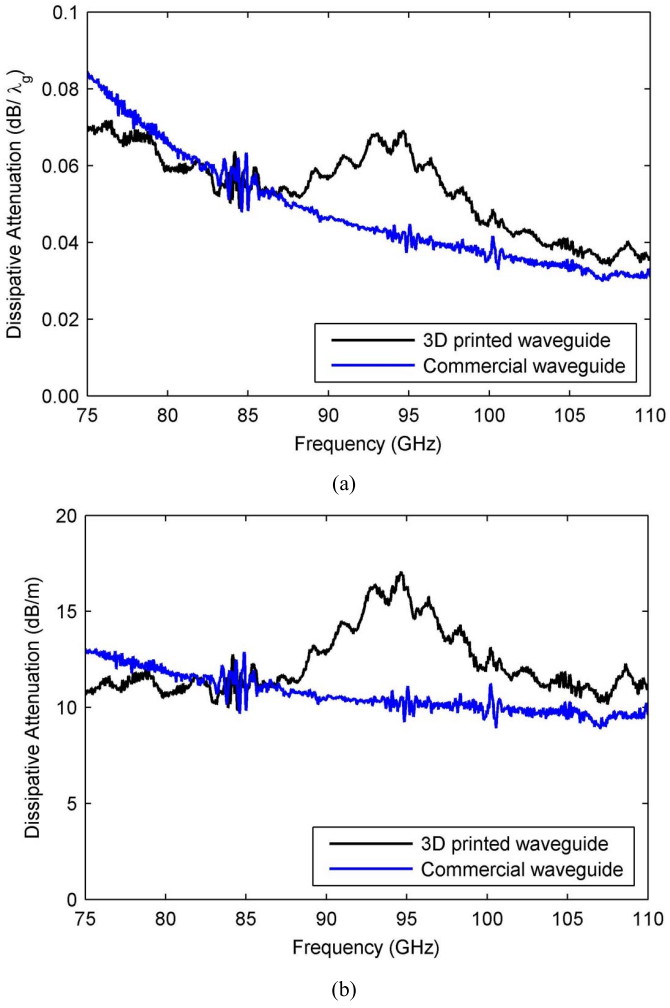

Fig. 9. Measured dissipative attenuation for the 60-mm length SLA printed waveguide with copper walls and 50-mm length commercial machined waveguides with aluminum walls (a) per guided wavelength and (b) per meter.

VII. W-BAND FILTER

In addition to forming feed lines and interconnects, MPRWG technology is also used for implementing critical passive components and networks. For example, high-quality (Q)-factor resonators are the basic building blocks for implementing high-performance filters. Most of the microwave and millimeter-wave bandpass filters that are currently manufactured are of the Chebyshev family, which has a transfer function that produces the best out-of-band rejection for a given maximum permitted level of passband equiripple insertion loss [76]. Narrow-band high-order conventional Chebyshev filters (e.g., sixth-order and higher) will have their return loss zeros distributed across an extremely small frequency range and, therefore, a very accurate manufacturing process needs to be employed [76]. For this reason, a sixth-order Chebyshev bandpass filter will demonstrate the advantage of 3-D printing over the micromolded and more expensive (micro)machined technologies.

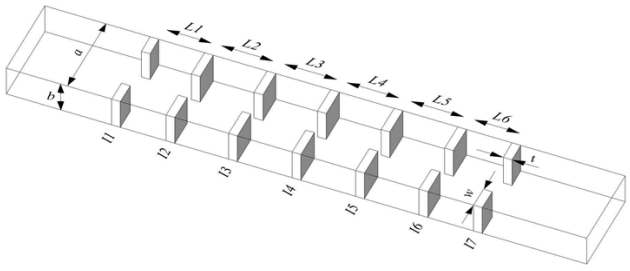

Fig. 10. Illustration of the sixth-order inductive iris bandpass filter. The associated design values are given in Table II, while the values measured after manufacture are given in Table III.

Here, an inductive iris bandpass filter implementation was chosen for the split-block solution, as shown in Fig. 10, so as to minimize misalignment effects. The filter was designed to have an arbitrary chosen center frequency of 100 GHz and a 3-dB bandwidth of 10 GHz.

The filter was designed using Guided Wave Technology (GWT) software that employs the mode-matching method [77]; iterations were needed to achieve spatial symmetry. It should be noted that an ideal manufacturing process is assumed (e.g., spatial features are perfectly rectangular, no mechanical misalignments and with perfect electrical conductor walls).

The minimum reliable thickness for an unplated iris wall was chosen; limited to approximately 140 μm, to maintain

TABLE II
FILTER DESIGN DIMENSIONS (ASSUMING IDEAL MANUFACTURING)

Plated Cavity Length, L (μm)		Plated Iris Width, w (μm)		
		Iris	*Left Side*	*Right Side*
L1	*1346*	*I1*	*583*	*583*
L2	*1551*	*I2*	*765*	*765*
L3	*1592*	*I3*	*809*	*809*
L4	*1592*	*I4*	*817*	*817*
L5	*1551*	*I5*	*809*	*809*
L6	*1346*	*I6*	*765*	*765*
		I7	*583*	*583*

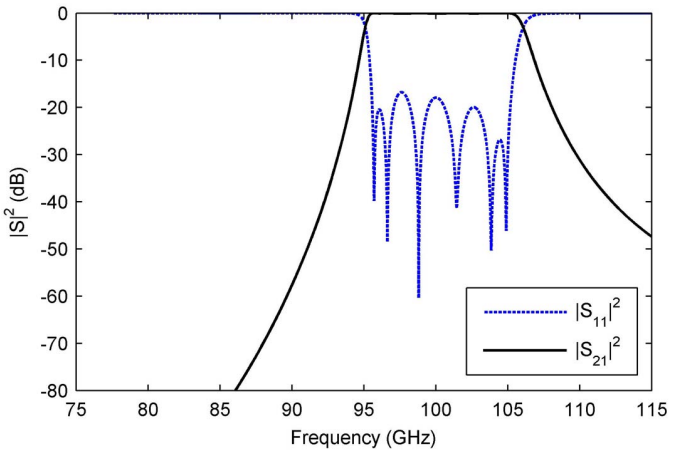

Fig. 11. Simulated S-parameters for the designed sixth-order Chebyshev filter with an ideal manufacturing process.

repeatability and tolerance control with SLA printing. In addition, the electroless and electroplating process was assumed to give a combined metal wall thickness of 30 μm, as found with the previously manufactured MPRWG thru line sections. The inductive iris thickness was, therefore, chosen to be $t = 200$ μm.

The final filter design dimensions were entered into the numerical 3-D modeling software CST Microwave Studio®, for verification; the values are given in Table II. Fig. 11 shows the simulated frequency response for the ideal bandpass filter. The six return loss zeros of the sixth-order Chebyshev filter can be clearly seen, with an associated predicted worst case in-band return loss of 18 dB.

Fig. 12 shows orthogonal cross sections through the filter structure, with the CAD layout and a single manufactured split-block part. The manufactured part appears to have no noticeable visual defects, when compared with the CAD layout.

The physical dimensions for the manufactured filter were measured using a scanning electron microscope and the results are given in Table III. From this data, it was found that there was an average shrinkage of 1.4% in the resin structure after final UV curing. This results in shorter cavity lengths, increasing the frequencies of the return loss zeros and, therefore, increasing the overall passband of the filter. In addition, the overall thickness of the metal wall was found

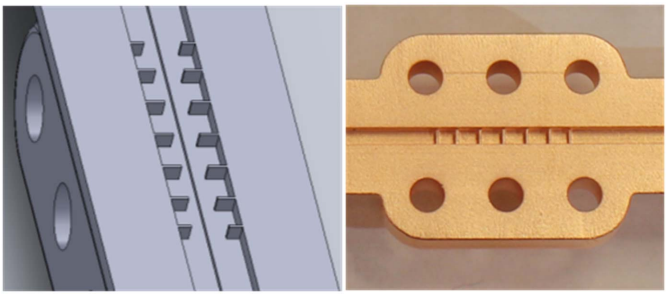

Fig. 12. W-band sixth-order filter. (a) CAD layout showing a horizontal cross section through both parts of the assembled split block. (b) Photograph of a single manufactured split-block part showing the vertical cross section.

TABLE III
MANUFACTURED FILTER DIMENSIONS

Plated Cavity Length, L (μm)			Width and thickness (μm)				
	Left side	*Right side*	*Iris*	*Left side*		*Right side*	
				w	*t*	*w*	*t*
L1	*1283*	*1278*	*I1*	*639*	*228*	*599*	*224*
L2	*1487*	*1489*	*I2*	*759*	*256*	*820*	*252*
L3	*1533*	*1513*	*I3*	*889*	*251*	*857*	*246*
L4	*1525*	*1513*	*I4*	*892*	*248*	*860*	*264*
L5	*1481*	*1459*	*I5*	*879*	*234*	*867*	*248*
L6	*1244*	*1242*	*I6*	*776*	*296*	*826*	*323*
			I7	*623*	*215*	*580*	*222*

Measured internal waveguide dimensions: $a = 2.51$ mm, $b = 1.25$ mm.

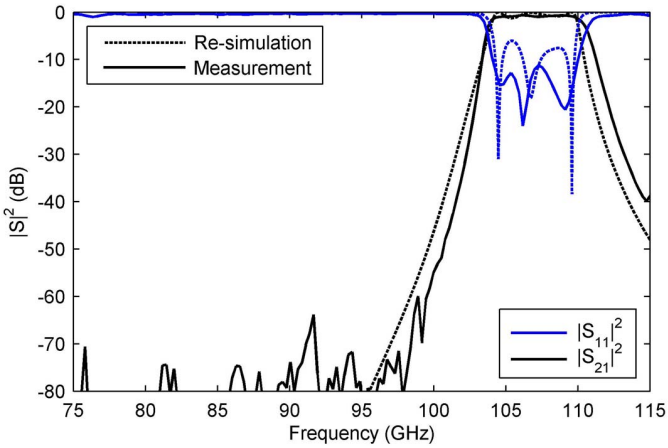

Fig. 13. Measured and resimulated S-parameters for the sixth-order 3-D printed W-band inductive iris bandpass filter.

to be overplated by 25 μm, on average, resulting in a total plated inductive iris thickness of 248 μm. With variable resin shrinkage and overplating, there will be slight asymmetries between the iris pairs associated with both split-block parts. This has the effect of slightly reducing the frequencies of the return loss zeros. However, the net effect of resin shrinkage, overplating and asymmetry is to increase the center frequency of the passband. Both internal and external cavity resonator coupling coefficients are directly proportional to the passband bandwidth [78]. Therefore, shrinkage and overplating also results in reduced cavity coupling and a decrease in passband bandwidth.

The S-parameter magnitudes for the manufactured filter, measured using traceable national standards at NPL, are given in Fig. 13. An excellent bandpass filter performance has been achieved, with a worst case passband return loss of 11 dB and insertion loss of 0.95 dB at the center frequency of 107.2 GHz. Clearly, the center frequency has been shifted up by 7.2% and the bandwidth has shrunk from 10 to 6.8 GHz with this first proof-of-principle demonstrator. With an optimized manufacturing process, design rules can be implemented to compensate for shrinkage and overplating.

The loaded quality factor for the filter Q_L is given by

$$Q_L(f_0) = \frac{f_0}{\Delta f} = 15.76 \tag{3}$$

where f_0 is the center frequency and Δf is the 3 dB bandwidth. The unloaded quality factor, Q_u, is obtained from the well-known relationship

$$Q_u(f_0) = \frac{Q_L(f_0)}{1 - |S_{21}(f_0)|} = 152. \tag{4}$$

The results for our sixth-order filter at 107.2 GHz can be favorably compared with those for the fifth-order filter fabricated using micromolding manufacturing technology: $Q_L(95.4\ \text{GHz}) = 27.27$ and $Q_u(95.4\ \text{GHz}) = 82$ [24], with almost twice the measured unloaded quality factor with our demonstrator.

Because the original design dimensions in Table II have changed to the actual physical dimensions in Table III, the measured S-parameters should be compared with resimulations based on the values in Table III. The results are shown in Fig. 13, indicating a good fit.

VIII. Conclusion

For the first time, this paper has investigated the manufacture of air-filled MPRWGs using 3-D printing technologies. Two very different technologies were considered: low-cost low-resolution FDM for microwave applications and high-cost high-resolution stereolithography for millimeter-wave applications.

Measurements against traceable standards in MPRWGs were performed by the U.K.'s NPL to provide confidence in the measured results. It was found that the performances of the 3-D printed MPRWGs were commensurate with those of commercial waveguides.

A high-performance W-band sixth-order inductive iris bandpass filter, having a center frequency of 107.2 GHz and a 6.8-GHz bandwidth, was also demonstrated. The measured insertion loss of the complete structure (filter, feed sections, and flanges) was only 0.95 dB at center frequency, giving an unloaded quality factor of 152—clearly demonstrating the potential of 3-D printed MPRWGs. This passive component fabrication technology offers the advantages of lightweight rapid prototyping/manufacturing, relatively very low cost, and potentially commensurate performance when compared with traditional (micro)machining.

Acknowledgment

The authors would like to thank Rapid 3-D Ltd for the manufacturing of the SLA printed parts and 3DDC Ltd for the electroless plating. They would also like to thank Dr. M. M. Ahmad, Dr. F. Hu, and J. Elsdon for their assistance. Finally, the financial assistance from Dr. K. Fobelets is gratefully appreciated.

References

[1] S. Lucyszyn, H. Q. Wang, and I. D. Robertson, "0.1 THz rectangular waveguide on GaAs semi-insulating substrate," *Electron. Lett.*, vol. 31, no. 9, pp. 721–722, Apr. 1995.

[2] S. Lucyszyn, D. Budimir, H. Q. Wang, and I. D. Robertson, "Design of compact monolithic dielectric-filled metal-pipe rectangular waveguides for millimetre-wave applications," *IEE Proc.-Microw., Antennas Propag.*, vol. 143, no. 5, pp. 451–453, Oct. 1996.

[3] M. S. Aftanasar, P. R. Young, I. D. Robertson, J. Minalgiene, and S. Lucyszyn, "Photoimageable thick-film millimetre-wave metal-pipe rectangular waveguides," *Electron. Lett.*, vol. 37, no. 18, pp. 1122–1123, Aug. 2001.

[4] S. Papantonis, N. M. Ridler, and S. Lucyszyn, "Rectangular waveguide enabling technology using holey surfaces and wire media metamaterials," *Sens. Actuators A, Phys.*, vol. 209, pp. 1–8, Mar. 2014.

[5] Y. Zhou and S. Lucyszyn, "Modelling of reconfigurable terahertz integrated architecture (RETINA) SIW structures," *Prog. Electromagn. Res.*, vol. 105, pp. 71–92, Jun. 2010.

[6] I. Stil, A. L. Fontana, B. Lefranc, A. Navarrini, P. Serres, and K. F. Schuster, "Loss of WR10 waveguide across 70–116 GHz," in *Proc. 22nd Int. Symp. Space Terahertz Technol.*, Apr. 2012, pp. 1–3.

[7] P. J. Chou and R. Siemann, "Measurements of losses in EDMed waveguides and in first W-band structure," Stanford Linear Accelerator Center (SLAC), Stanford, CA, USA, Tech. Rep. ARDB-99, Jun. 1997.

[8] W. R. McGrath, C. Walker, M. Yap, and Y.-C. Tai, "Silicon micromachined waveguides for millimeter-wave and submillimeter-wave frequencies," *IEEE Microw. Guided Wave Lett.*, vol. 3, no. 3, pp. 61–63, Mar. 1992.

[9] S. Lucyszyn, "The future of on-chip terahertz metal-pipe rectangular waveguides implemented using micromachining and multilayer technologies," in *Proc. IEE Colloq. Terahertz Technol. Appl.*, Apr. 1997, pp. 10/1–10/10.

[10] K. M. K. H. Leong *et al.*, "WR1.5 silicon micromachined waveguide components and active circuit integration methodology," *IEEE Trans. Microw. Theory Techn.*, vol. 60, no. 4, pp. 998–1005, Apr. 2012.

[11] E. Episkopou, S. Papantonis, and S. Lucyszyn, "Optically-controlled plasma switch for integrated terahertz applications," in *Proc. IEEE Int. Conf. Plasma Sci. (ICOPS)*, Jul. 2012, p. 3P-43.

[12] T. J. Reck, C. Jung-Kubiak, J. Gill, and G. Chattopadhyay, "Measurement of silicon micromachined waveguide components at 500–750 GHz," *IEEE Trans. Terahertz Sci. Technol.*, vol. 4, no. 1, pp. 33–38, Jan. 2014.

[13] S. W. Moon *et al.*, "Terahertz waveguide components fabricated using a 3D X-ray microfabrication technique," *Electron. Lett.*, vol. 32, no. 19, pp. 1794–1795, Sep. 1996.

[14] J. W. Digby *et al.*, "Integrated micro-machined antenna for 200 GHz operation," in *Proc. IEEE MTT-S Int. Microw. Symp.*, vol. 2. Jun. 1997, pp. 561–564.

[15] C. E. Collins *et al.*, "Micro-machined 'snap-together' rectangular waveguide for terahertz circuits," in *Proc. IEEE 6th Int. Conf. Terahertz Electron.*, Sep. 1998, pp. 176–178.

[16] J. W. Digby *et al.*, "Fabrication and characterization of micromachined rectangular waveguide components for use at millimeter-wave and terahertz frequencies," *IEEE Trans. Microw. Theory Techn.*, vol. 48, no. 8, pp. 1293–1302, Aug. 2000.

[17] J. W. Bowen *et al.*, "Micromachined waveguide antennas for 1.6 THz," *Electron. Lett.*, vol. 42, no. 15, pp. 842–843, Jul. 2006.

[18] C. H. Smith, A. Sklavonuos, and N. S. Barker, "SU-8 micromachining of millimeter and submillimeter waveguide circuits," in *IEEE MTT-S Int. Microw. Symp. Dig.*, Jun. 2009, pp. 961–964.

[19] N. A. Murad, M. J. Lancaster, P. Gardner, M. L. Ke, and Y. Wang, "Micromachined H-plane horn antenna manufactured using thick SU-8 photoresist," *Electron. Lett.*, vol. 46, no. 11, pp. 743–745, May 2010.

[20] X. Shang, M. L. Ke, Y. Wang, and M. J. Lancaster, "Micromachined WR-3 waveguide filter with embedded bends," *Electron. Lett.*, vol. 47, no. 9, pp. 545–547, Apr. 2011.

[21] X. Shang, M. L. Ke, Y. Wang, and M. J. Lancaster, "WR-3 band waveguides and filters fabricated using SU8 photoresist micromachining technology," *IEEE Trans. Terahertz Sci. Technol.*, vol. 2, no. 6, pp. 629–637, Nov. 2012.

[22] X. Shang, Y. Tian, M. J. Lancaster, and S. Singh, "A SU8 micromachined WR-1.5 band waveguide filter," *IEEE Microw. Wireless Compon. Lett.*, vol. 23, no. 6, pp. 300–302, Jun. 2013.

[23] F. Sammoura *et al.*, "Plastic 95-GHz rectangular waveguides by micro molding technologies," *Sens. Actuators A, Phys.*, vol. 127, no. 2, pp. 270–275, Mar. 2006.

[24] F. Sammoura, Y. Cai, C.-Y. Chi, T. Hirano, L. Lin, and J.-C. Chiao, "A micromachined W-band iris filter," in *Proc. 13th Int. Conf. Solid-State Sens., Actuators Microsyst.*, vol. 1. Jun. 2005, pp. 1067–1070.

[25] C. Reilly *et al.*, "New fabrication technology for ceramic metamaterials," in *Proc. IEEE Antennas Propag. Soc. Int. Symp.*, vol. 2. Jun. 2002, pp. 376–379.

[26] W. J. Chappell, C. Reilly, J. Halloran, and L. P. B. Katehi, "Ceramic synthetic substrates using solid freeform fabrication," *IEEE Trans. Microw. Theory Techn.*, vol. 51, no. 3, pp. 752–760, Mar. 2003.

[27] X. Gong, B. Liu, L. P. B. Katehi, and W. J. Chappell, "Layer-by-layer stereolithography (SL) of complex medium," in *Proc. IEEE Antennas Propag. Soc. Int. Symp.*, vol. 1. Jun. 2004, pp. 325–328.

[28] B. Liu, X. Gong, and W. J. Chappell, "Layer-by-layer polymer stereolithography fabrication for three-dimensional RF components," in *IEEE MTT-S Int. Microw. Symp. Dig.*, vol. 2. Jun. 2004, pp. 481–484.

[29] X. Gong, A. Margomenos, B. Liu, W. J. Chappell, and L. P. B. Katehi, "High-Q evanescent-mode filters using silicon micromachining and polymer stereolithography (SL) processing," in *IEEE MTT-S Int. Microw. Symp. Dig.*, vol. 2. Jun. 2004, pp. 433–436.

[30] B. Liu, X. Gong, and W. J. Chappell, "Applications of layer-by-layer polymer stereolithography for three-dimensional high-frequency components," *IEEE Trans. Microw. Theory Techn.*, vol. 52, no. 11, pp. 2567–2575, Nov. 2004.

[31] Y. Huang, X. Gong, S. Hajela, and W. J. Chappell, "Layer-by-layer stereolithography of three-dimensional antennas," in *Proc. IEEE Antennas Propag. Soc. Int. Symp.*, vol. 1A. Jul. 2005, pp. 276–279.

[32] A. Buerkle, K. F. Brakora, and K. Sarabandi, "Fabrication of a DRA array using ceramic stereolithography," *IEEE Antennas Wireless Propag. Lett.*, vol. 5, no. 1, pp. 479–482, Dec. 2006.

[33] K. F. Brakora, J. Halloran, and K. Sarabandi, "Design of 3-D monolithic MMW antennas using ceramic stereolithography," *IEEE Trans. Antennas Propag.*, vol. 55, no. 3, pp. 790–797, Mar. 2007.

[34] K. Brakora, J. Halloran, and K. Sarabandi, "Subwavelength periodic lattices for the design of MMW components using ceramic stereolithography," in *Proc. IEEE Antennas Propag. Soc. Int. Symp.*, Jul. 2006, pp. 4511–4514.

[35] K. F. Brakora and K. Sarabandi, "Integration of single-mode photonic crystal clad waveguides with monolithically constructed ceramic subsystems," *IEEE Antennas Wireless Propag. Lett.*, vol. 8, pp. 433–436, Aug. 2008.

[36] K. F. Brakora and K. Sarabandi, "Integration of single-mode photonic crystal waveguides to monolithic MMW subsystems constructed using ceramic stereolithography," in *Proc. IEEE Antennas Propag. Soc. Int. Symp.*, Jun. 2007, pp. 2550–2553.

[37] N. Delhote, D. Baillargeat, S. Verdeyme, C. Delage, and C. Chaput, "Narrow Ka bandpass filters made of high permittivity ceramic by layer-by-layer polymer stereolithography," in *Proc. 36th Eur. Microw. Conf. (EuMC)*, Sep. 2006, pp. 510–513.

[38] N. Delhote, D. Baillargeat, S. Verdeyme, C. Delage, and C. Chaput, "Ceramic layer-by-layer stereolithography for the manufacturing of 3-D millimeter-wave filters," *IEEE Trans. Microw. Theory Techn.*, vol. 55, no. 3, pp. 548–554, Mar. 2007.

[39] T. Chartier *et al.*, "Fabrication of millimeter wave components via ceramic stereo- and microstereolithography processes," *J. Amer. Ceram. Soc.*, vol. 91, no. 8, pp. 2469–2474, Aug. 2008.

[40] N. T. Nguyen, N. Delhote, M. Ettorre, D. Baillargeat, L. Le Coq, and R. Sauleau, "Design and characterization of 60-GHz integrated lens antennas fabricated through ceramic stereolithography," *IEEE Trans. Antennas Propag.*, vol. 58, no. 8, pp. 2757–2762, Aug. 2010.

[41] Y. Lee *et al.*, "Rapid prototyping of ceramic millimeterwave metamaterials: Simulations and experiments," *Microw. Opt. Technol. Lett.*, vol. 49, no. 9, pp. 2090–2093, Sep. 2007.

[42] C. R. Garcia *et al.*, "3D printing of anisotropic metamaterials," *Prog. Electromagn. Res. Lett.*, vol. 34, pp. 75–82, Jul. 2012.

[43] Y. Urzhumov, N. Landy, T. Driscoll, D. Basov, and D. R. Smith, "Thin low-loss dielectric coatings for free-space cloaking," *Opt. Lett.*, vol. 38, no. 10, pp. 1606–1608, May 2013.

[44] L. Schulwitz and A. Mortazawi, "A compact millimeter-wave horn antenna array fabricated through layer-by-layer stereolithography," in *Proc. IEEE Antennas Propag. Soc. Int. Symp.*, Jul. 2008, pp. 1–4.

[45] P. T. Timbie, J. Grade, D. van der Weide, B. Maffei, and G. Pisano, "Stereolithographed MM-wave corrugated horn antennas," in *Proc. 36th Int. Conf. Infr., Millim. Terahertz Waves*, Oct. 2011, pp. 1–3.

[46] W. G. Whittow, C. C. Njoku, and J. C. Vardaxoglou, "Patch antennas with heterogeneous substrates and reduced material consumption enabled by additive manufacturing techniques," in *Proc. IEEE Antennas Propag. Soc. Int. Symp.*, Jul. 2012, p. 244.

[47] W. G. Whittow, S. S. Bukhari, L. A. Jones, and I. L. Morrow, "Applications and future prospects for microstrip antennas using heterogeneous and complex 3-D geometry substrates," *Prog. Electromagn. Res.*, vol. 144, pp. 271–280, Jan. 2014.

[48] J. W. Allen and B.-I. Wu, "Design and fabrication of an RF GRIN lens using 3D printing technology," *Proc. SPIE*, vol. 8624, p. 86240V, Mar. 2013.

[49] M. Liang, W.-R. Ng, K. Chang, K. Gbele, M. E. Gehm, and H. Xin, "A 3-D Luneburg lens antenna fabricated by polymer jetting rapid prototyping," *IEEE Trans. Antennas Propag.*, vol. 62, no. 4, pp. 1799–1807, Apr. 2014.

[50] B. Sanz-Izquierdo and E. A. Parker, "3-D printing of elements in frequency selective arrays," *IEEE Trans. Antennas Propag.*, vol. 62, no. 12, pp. 6060–6066, Dec. 2014.

[51] Z. Wu, J. Kinast, M. E. Gehm, and H. Xin, "Rapid and inexpensive fabrication of terahertz electromagnetic bandgap structures," *Opt. Exp.*, vol. 16, no. 21, pp. 16442–16451, Oct. 2008.

[52] Z. Wu, W.-R. Ng, M. E. Gehm, and H. Xin, "Terahertz electromagnetic crystal waveguide fabricated by polymer jetting rapid prototyping," *Opt. Exp.*, vol. 19, no. 5, pp. 3962–3972, Feb. 2011.

[53] S. Pandey, B. Gupta, and A. Nahata, "Terahertz plasmonic waveguides created via 3D printing," *Opt. Exp.*, vol. 21, no. 21, pp. 24422–24430, Oct. 2013.

[54] N. Yudasari, D. Vogt, J. Anthony, and R. Leonhardt, "Hollow core terahertz waveguide fabricated using a 3D printer," in *Proc. 39th Int. Conf. Infr., Millim., Terahertz Waves (IRMMW-THz)*, vol. 2. Sep. 2014, pp. 1–2.

[55] P. Nayeri *et al.*, "3D printed dielectric reflectarrays: Low-cost high-gain antennas at sub-millimeter waves," *IEEE Trans. Antennas Propag.*, vol. 62, no. 4, pp. 2000–2008, Apr. 2014.

[56] A. Macor, E. de Rijk, S. Alberti, T. Goodman, and J.-P. Ansermet, "Note: Three-dimensional stereolithography for millimeter wave and terahertz applications," *Rev. Sci. Instrum.*, vol. 83, no. 4, p. 046103, Apr. 2012.

[57] A. von Bieren, E. de Rijk, J.-P. Ansermet, and A. Macor, "Monolithic metal-coated plastic components for mm-wave applications," in *Proc. 39th Int. Conf. Infr., Millim., Terahertz Waves (IRMMW-THz)*, vol. 1. Sep. 2014, pp. 1–2.

[58] Swissto12. *Metal Coated Plastics*. [Online]. Available: http://www.swissto12.com/Products/Metal Coated Plastics/index.html, accessed May 8, 2015.

[59] S. S. Crump, "Modeling apparatus for three-dimensional objects," U.S. Patent 5 340 433, Jun. 8, 1992.

[60] C. W. Hull, "Apparatus for production of three-dimensional objects by stereolithography," U.S. Patent 4 575 330, Aug. 8, 1984.

[61] C. R. Deckard, "Method and apparatus for producing parts by selective sintering," U.S. Patent 4 863 538, Oct. 17, 1986.

[62] N. Hopkinson and P. Dicknes, "Analysis of rapid manufacturing—Using layer manufacturing processes for production," *Proc. Inst. Mech. Eng. C, J. Mech. Eng. Sci.*, vol. 217, no. 1, pp. 31–39, Jan. 2003.

[63] A. Weber. (Aug. 2013). Case study: Kelly Manufacturing Company—A turn for the better. Stratasys, Rehovot, Israel. [Online]. Available: http://www.stratasys.com/resources/case-studies/aerospace/kelly-manufacturing

[64] G. Schmidt and U. Eidenschink. (Jul. 2013). Case study: BMW Regensburg—Rapid manufacturing with FDM in jig & fixture construction. Stratasys, Rehovot, Israel. [Online]. Available: http://www.stratasys.com/resources/case-studies/automotive/bmw

[65] A. Rutter and V. Sharma. (Nov. 2014). Low volume, agile, additive manufacturing and capital costs. Type A Machines, San Francisco, CA, USA. [Online]. Available: http://www.typeamachines.com/pages/white-paper

[66] A. Kreemer and Z. H. Moe, "Rapid manufacturing using FDM systems," in *Handbook of Manufacturing Engineering and Technology*, A. Nee, Ed. London, U.K.: Springer-Verlag, 2014, pp. 1–11.
[67] G. O. Mallory and J. B. Hajdu, Eds., *Electroless Plating: Fundamentals and Applications*. Orlando, FL, USA: Noyes Publications/William Andrew Publishing, 1990.
[68] *Waveguide Loss*. [Online]. Available: http://www.microwaves101.com/encyclopedias/waveguide-loss, accessed May 15, 2015.
[69] *Accura Xtreme Plastic Datasheet*. [Online]. Available: http://www.3dsystems.com/products/datafiles/datasheets/SLA/DS_Accura_Xtreme_US.pdf, accessed Feb. 19, 2015.
[70] *Assessment of Surface Texture. Guidance and General Information*, British Standard BS 1134:2010, 2010.
[71] G. F. Engen and C. A. Hoer, "Thru-reflect-line: An improved technique for calibrating the dual six-port automatic network analyzer," *IEEE Trans. Microw. Theory Techn.*, vol. 27, no. 12, pp. 987–993, Dec. 1979.
[72] A. Rumiantsev and N. M. Ridler, "VNA calibration," *IEEE Microw. Mag.*, vol. 9, no. 3, pp. 86–99, Jun. 2008.
[73] N. M. Ridler, "News in RF impedance measurements," in *Proc. 27th General Assembly Int. Union Radio Sci. (URSI)*, 2002, paper 374.
[74] N. M. Ridler, "A review of existing national measurement standards for RF and microwave impedance parameters in the UK," in *IEE Colloq. Dig.*, Feb. 1999, pp. 6/1–6/6.
[75] F. L. Warner, "Attenuation measurement," in *Microwave Measurements*, A. E. Bailey, Ed., 2nd ed. London, U.K.: IEE, 1989, pp. 132–134.
[76] C. E. Chrisostomidis and S. Lucyszyn, "On the theory of chained-function filters," *IEEE Trans. Microw. Theory Techn.*, vol. 53, no. 10, pp. 3142–3151, Oct. 2005.
[77] Guided Wave Technology (GTW). *Online Microwave Filter Design—Iris Filter*. [Online]. Available: http://www.guidedwavetech.com/wgchoose.htm, accessed Aug. 6, 2015.
[78] A. Poithier and T. Vaha-Heikkila, "Impedance tuners and tuneable filters," in *Advanced RF MEMS*, S. Lucyszyn, Ed. Cambridge, U.K.: Cambridge Univ. Press, 2010, pp. 271–306.

Mario D'Auria (S'11) received the M.Sc. degree in electronics engineering from the Second University of Naples, Naples, Italy, in 2010. He is currently pursuing the Ph.D. degree with Imperial College London, London, U.K.

His current research interests include LTCC, silicon laser micromachining, and 3-D printing for RF and microwave applications.

William J. Otter (S'12–M'15) received the M.Eng. degree in electrical and electronic engineering and the Ph.D. degree from Imperial College London, London, U.K., in 2010 and 2015, respectively.

He undertook industrial placements with BAE Systems, Advanced Technology Centre, Great Baddow, U.K., during the M.Eng. degree, and held the Val O'Donoghue Scholarship from the Department of Electrical and Electronic Engineering thorughout the Ph.D. degree. He is currently a Research Associate with Imperial College London, where he is involved in millimeter-wave and terahertz sensor design. His current research interests include photonic crystals, low-cost terahertz devices, electromagnetic modeling, filter design, optoelectronics, and terahertz and microwave sensors.

Jonathan Hazell received the M.Eng. degree in electrical and electronic engineering from Imperial College London, London, U.K., in 2012, where he is currently pursuing the Ph.D. degree in high frequency vacuum electronics.

His current research interests include traveling wave tubes, terahertz filters, and novel manufacturing techniques.

Brendan T. W. Gillatt, photograph and biography not available at the time of publication.

Callum Long-Collins, photograph and biography not available at the time of publication.

Nick M. Ridler (M'03–SM'05–F'14) is currently a Principal Research Scientist with the National Physical Laboratory, Middlesex, U.K. He is a Visiting Professor with the School of Electronic and Electrical Engineering, Faculty of Engineering, University of Leeds, Leeds, U.K., and the Faculty of Engineering and Physical Sciences, University of Surrey, Surrey, U.K. His current research interests include high-frequency precision electromagnetic measurement.

Prof. Ridler is a fellow of the Institution of Engineering and Technology in U.K. and a Chartered Engineer. He holds a Fellowship from the Advanced Technology Institute, University of Surrey. He is the Chair of the IEEE MTT Society Administrative Committee's Standards Coordinating Committee and the IEEE Standard Working Group P1785 Waveguide for Millimeter and Submillimeter Wavelengths, and the Vice Chair of the IEEE Standard Working Group P287 Precision Coaxial Connectors at RF, Microwave and Millimeter-Wave Frequencies. He was the President of the Automatic RF Techniques Group and the Emeritus Chair of the IEEE MTT-11 Microwave Measurements Technical Committee. He represents the International Electrotechnical Commission on the International Bureau of Weights and Measures Joint Committee for Guides in Metrology Working Group 1 "Expression of Uncertainty in Measurement (GUM)."

Stepan Lucyszyn (M'91–SM'04–F'14) received the Ph.D. degree in electronics engineering from King's College London, London, U.K., in 1992, and the D.Sc. (higher doctorate) degree in millimeter-wave and terahertz electronics from Imperial College London, London, U.K., in 2010.

He co-founded Drayson Wireless Ltd., a spin-out company of Imperial College London, in 2014. He is currently a Reader (Associate Professor) in Millimeter-Wave Electronics and Director of the Centre for Terahertz Science and Engineering within Imperial College London. He has co-authored over 180 papers and 12 book chapters in applied physics and electronic engineering.

Dr. Lucyszyn has been a fellow of the Institute of Physics in U.K. since 2005, the Institution of Engineering and Technology in U.K. since 2005, and The Electromagnetics Academy in USA since 2008. He was an Associate Editor of the IEEE JOURNAL OF MICROELECTROMECHANICAL SYSTEMS from 2005 to 2009. In 2011, he was the Chairman of the 41st European Microwave Conference, Manchester, U.K, and will be the Co-Chair of the 11th European Microwave Integrated Circuits Conference in London in 2016. He was an IEEE Distinguished Microwave Lecturer (DML) from 2010 to 2012, and an Emeritus DML in 2013. He has been an EuMA European Microwave Lecturer since 2013. He has delivered many invited presentations at international conferences.